The RNA-binding protein HuR impairs adipose tissue anabolism in pancreatic cancer cachexia

Paige C. Arneson-Wissink[1,2], Katherine Pelz[1,3], Beth Worley[1], Heike Mendez [1,2], Peter Pham [1,2], Grace McCarthy [1,3], Alex Chitsazan[4], Jonathan R. Brody [1,3,5], Aaron J. Grossberg*[1,2,4,5]

[1]Brenden-Colson Center for Pancreatic Care, Oregon Health & Science University, Portland, OR

[2]Department of Radiation Medicine, Oregon Health & Science University, Portland, OR

[3]Department of Surgery, Oregon Health & Science University, Portland, OR

[4]Cancer Early Detection Advanced Research Center, Oregon Health & Science University, Portland, OR

[5]Department of Cell, Developmental, and Cancer Biology, Oregon Health & Science University, Portland, OR

***Corresponding Author**: Aaron J. Grossberg, 3181 SW Sam Jackson Park Rd Mail Code L481, Oregon Health and Science University, Portland, OR, 97239, 503-494-9945, grossber@ohsu.edu

ABSTRACT

Background: Cachexia is defined by chronic loss of fat and muscle, is a frequent complication of pancreatic ductal adenocarcinoma (PDAC), and negatively impacts patient outcomes. Nutritional supplementation cannot fully reverse tissue wasting, and the mechanisms underlying this phenotype are unclear. This work aims to define the relative contributions of catabolism and anabolism to adipose wasting in PDAC-bearing mice. Human antigen R (HuR) is an RNA-binding protein recently shown to suppress adipogenesis. We hypothesize that fat wasting results from a loss of adipose anabolism driven by increased HuR activity in adipocytes of PDAC-bearing mice.

Methods: Adult C57BL/6J mice received orthotopic PDAC cell (*Kras^{G12D}; p53$^{R172H/+}$; Pdx1-cre*) (OT-PDAC) or PBS (sham) injections. Mice exhibiting moderate cachexia (9 days after injection) were fasted for 24h, or fasted 24h and refed 24h before euthanasia. A separate cohort of PDAC mice were treated with an established HuR inhibitor (KH-3, 100 mg/kg) and subjected to the fast/refeed paradigm. We analyzed body mass, gross fat pad mass, and adipose tissue mRNA expression. We quantified lipolytic rate as the normalized quantity of glycerol released from 3T3-L1 adipocytes *in vitro*, and gonadal fat pads (gWAT) *ex vivo*.

Results: 3T3-L1 adipocytes treated with PDAC cell conditioned media (CM) liberated less triglyceride into the culture media than control-treated adipocytes (-28.1%) and had lower expression of lipolysis and lipogenesis genes than control cells. PDAC gWAT cultured *ex vivo* displayed decreased lipolysis compared to sham gWAT (-54.7%). PDAC and sham mice lost equivalent fat mass after a 24h fast, however, PDAC mice could not restore inguinal fat pads (iWAT) (-40.5%) or gWAT (-31.8%) mass after refeeding. RNAseq revealed 572 differentially expressed genes in gWAT from PDAC compared to sham mice. Downregulated genes

(n=126) were associated with adipogenesis (adj p=0.05), and expression of adipogenesis master regulators *Pparg* and *Cebpa* were reduced in gWAT from PDAC mice. Immunohistochemistry revealed increased HuR staining in gWAT (+74.9%) and iWAT (+41.2%) from PDAC mice. Inhibiting HuR binding restored lipogenesis in refed animals with a concomitant increase in iWAT mass (+131.7%) and genes regulating adipogenesis (*Pparγ*, *Cebpa*, *Retn*, *Adipoq*, *Fasn*).

Conclusions: Our work highlights deficient adipose anabolism as a driver of wasting in 3T3-L1 adipocytes treated with PDAC conditioned media and OT-PDAC mice. The small molecule KH3, which disrupts HuR binding, was sufficient to restore adipogenic and lipogenic gene expression and prevent adipose wasting. This highlights HuR as a potentially targetable regulatory node for adipose anabolism in cancer cachexia.

Key words: pancreatic ductal adenocarcinoma, cachexia, adipose, adipogenesis, HuR

INTRODUCTION

Cancer-associated cachexia is a wasting condition characterized by systemic inflammation, progressive weight loss, and atrophy of white adipose tissue (WAT) and skeletal muscle[1-3]. In addition to physical deterioration, individuals with cachexia also exhibit fatigue, anorexia, and cognitive decline[1-4], which contribute significantly to reductions in quality of life, ability to tolerate chemotherapy or surgery, and patient mortality[5-9]. Cachexia is estimated to be the direct cause of death in 20-30% of cancer patients[5, 6], and among all malignancies, pancreatic ductal adenocarcinoma (PDAC) is the most highly associated with cachexia, with an estimated 83% of patients suffering from this condition[10-12]. Despite much of cachexia research focusing on improving skeletal muscle mass, a retrospective study of patients with PDAC revealed that fat loss alone is associated with equally poor outcomes as combined muscle and fat mass loss [13]. Additionally, current cachexia clinical trials center around weight maintenance or gain as a primary endpoint. This highlights the importance of understanding the drivers of adipose tissue loss in cachexia.

Cachexia arises when energy catabolism exceeds anabolism, leading to unsustainable levels of fat mobilization and muscle depletion. Multiple factors are known to enhance catabolism, including decreased secretion of anabolic hormones, and altered metabolism of protein, carbohydrate, and lipid substrates[14]. Current work suggests that inflammation drives metabolic abnormalities in cachexia[10, 15]. Pro-inflammatory cytokine activity increases during cancer progression[16, 17] and systemic inflammation can contribute to wasting by inducing hypercatabolism in muscle and adipose tissue [14, 18-20]. Existing literature highlights elevated rates of lipolysis and adipose browning as the primary forces underlying adipose tissue wasting [21, 22]. Browning, in particular, appears to exert a double effect in

cachexia by both reducing lipid stores and increasing energy expenditure[22]. However, impaired anabolic processes, like adipogenesis and lipogenesis, also contribute to adipose tissue loss [23]. Targeting peroxisome proliferator-activated receptor gamma (PPARG), a transcriptional control point of adipogenesis, with the agonist rosiglitazone was sufficient to improve fat and muscle mass retention in mice with lung cancer [24]. Tumor-derived factors are also capable of impairing adipogenesis in cultured 3T3L-1 adipocytes [25, 26].

RNA-binding proteins (RBPs) are essential in governing biogenesis, stabilization, translation, and decay of mRNA transcripts[27, 28]. Several RBPs regulate alternative splicing in adipocytes[29-31] and promote white adipose tissue browning [32] by inhibiting the translation efficiency of mitochondrial mRNAs such as UCP1[33]. Until recently, the function of most RBPs in adipocytes was largely unexplored. Recent work demonstrated that the RBP human antigen R (HuR), encoded by the embryonic lethal abnormal vision-like 1 (*ELAVL1*) gene, which regulates the expression of genes involved in inflammation, stress response, and apoptosis, is also a repressor of adipogenesis in both white and brown adipose tissues[34, 35]. Our goal was to elucidate the relative contributions of enhanced catabolism and impaired anabolism on fat wasting by investigating adipose tissue response to different nutritional contexts and HuR inhibition in cachectic mice.

METHODS

Cell culture

KPC PDAC cells

KPC cells expressing pancreas-specific conditional alleles (*Kras^{G12D}; p53$^{R172H/+}$; Pdx1-cre*)[36] were stored in liquid nitrogen until use and then maintained in RMPI 1640 supplemented with 10% FBS, 1mM sodium pyruvate, and 50 U/mL penicillin/streptomycin

(Gibco, Gaithersburg, MD) at 37C and 5% CO_2. Conditioned media (CM) was collected from confluent KPC cells grown in DMEM, 1% pen/strep (to accommodate later culturing of 3T3-L1 cells) after 24 hours incubation, centrifuged at 1,200 g for 10 min, filtered with a 0.2-μm syringe filter, and used immediately or stored at −80°C.

3T3-L1 adipocytes

3T3-L1 adipocytes (ATCC CL-173) were purchased from ATCC and stored in liquid nitrogen until use. Cells were first treated with preadipocyte expansion media (DMEM, 10% bovine calf serum, 1% pen/strep) for 3-4 days. Then, cells were plated at a density of $2x10^5$ cells/6-well dish, or $6.7\ x10^3$ cells/96well dish and maintained in preadipocyte expansion media for 2 days after reaching 100% confluency. Media was changed to adipocyte differentiation media (DMEM, 10% FBS, 1% pen/strep, 1 uM dexamethasone, 0.5 mM IBMX, 1 ug/mL bovine insulin) for 2 days before switching to adipocyte maintenance media (DMEM, 10% FBS, 1% pen/strep, 1 ug/mL bovine insulin) for the duration of the experiment. Cells were cultured for up to 6 days after start of maintenance media. CM was added in place of adipocyte maintenance media and was supplemented with FBS and insulin.

Oil red O staining

Diluted Oil Red O stock solution was prepared by mixing concentrated Oil Red O (0.5% Oil Red O in 100% isopropyl alcohol) 6:4 with deionized water. This solution was allowed to stand for 10 minutes at 4C and then filtered immediately before use through a 0.22 um filter. 3T3-L1 cells were washed with PBS, then incubated in 4% paraformaldehyde for 30 minutes at room temperature, then washed with deionized water twice. Cells were incubated in 60% isopropyl alcohol for 5 minutes, then treated with diluted Oil Red O solution for 15 minutes.

Cells were washed 5 times with deionized water, then red signal was quantified at 490 nm in a plate reader (BioTek).

Triglyceride quantification

3T3-L1 mature adipocytes were treated with KPC CM or control media for 24 hours, then media was collected off of 3T3-L1 cells for triglyceride quantification according to manufacturer instructions (Stanbio Liquicolor Triglycerides Assay #2100, Fisher Scientific). Absorbance was read at 500 nm on a plate reader (BioTek).

Mouse studies

Wildtype C57BL/6J mice (JAX catalog number 000664) were purchased from The Jackson Laboratory (Bar Harbor, ME) and maintained in standard rodent housing at 26°C with 12h light/12h dark cycles. Animals used for experimentation were 12-15 weeks of age. Mice were individually housed for acclimation for 7 days prior to tumor implantation and provided *ad libitum* access to water and food (Rodent diet 5001; Purina Mills, St. Louis, MO, USA). Food intake was measured daily. Tumor-bearing animals were euthanized by cardiac puncture under deep isoflurane anesthesia. Studies were conducted in accordance with the U.S. National Institutes of Health Guide for the Care and Use of Laboratory Animals and approved by the Institutional Animal Care and Use Committee of Oregon Health & Science University.

Study-specific manipulations

For fasting studies, mice were transferred to clean cages without food for 24 hours prior to euthanasia or refeeding. Pair-feeding was used on the study days indicated in the figure legends by feeding sham mice the average of the food consumed by PDAC mice the day prior. PDAC mice treated with the HuR inhibitor KH3, were injected intraperitoneally (100 mg/kg) at 6-, 8-, and 10-days post-implantation.

Orthotopic PDAC implantation

Wildtype C57BL/6J mice aged 12-15 weeks received orthotopic PDAC tumor injections (*Kras^{G12D}; p53$^{R172H/+}$; Pdx1-cre*) or sham injections. PDAC mice were injected with 1x10^{6} KPC cells into the tail of the pancreas parenchyma in a volume of 23ul while sham animals were treated with an equal volume of PBS. Animals were euthanized 10-11 days after tumor implantation. N and sex are defined on a per-study basis in the figure legends.

Echo magnetic resonance imaging body composition

Lean mass, fat mass, total body water, and free water were measured using whole-body magnetic resonance imaging (MRI) (EchoMRI, Houston, TX). Measurements were taken pre-implantation, pre-fasting and at euthanasia in tumor and sham groups to assess body composition.

Tissue collection and histology

Tissues collected at necropsy were weighed and flash frozen in liquid nitrogen prior to storage at -80C. Tissues for HuR histology were fixed with 4% paraformaldehyde overnight and then transferred to 70% ethanol. Tissues were paraffin-embedded, sectioned, incubated with anti-HuR (1:300 #sc-5261, Santa Cruz Biotechnology Inc, Dallas, TX) and stained using horseradish peroxidase-conjugated secondary antibody and incubation in 3,3'-diaminobenzidine by the Histopathology Shared Resource Core at OHSU. Whole tissue sections were scanned by the Advanced Light Microscopy Core at OHSU. ZEN Digital Imaging for Light Microscopy (RRID:SCR_013672) was then used to obtain at least five 10x images per tissue. ImageJ software was used to quantify the percent staining for each section (56). All staining was quantified by running color deconvolution on 10x images, applying a standard

intensity threshold on the corresponding images, and measuring the percent area covered by the staining.

Ex vivo lipolysis

Ex vivo lipolysis assays of adipose explants were performed as previously described[37]. Briefly, gonadal white adipose tissue (gWAT) tissue was collected and cut into approximately 100 mg samples, minced, then incubated in phenol red-free DMEM containing 2% fatty acid free bovine serum albumin at 37°C for 1 hour. Media was collected and snap-frozen. The tissue was transferred to a new dish containing media only or media with 10 uM isoproterenol and incubated for 2 hours at 37C. Media was collected and snap-frozen. Media aliquots were thawed and analyzed for glycerol using Sigma Glycerol Assay Kit (MAK117) according to manufacturer's directions.

Quantitative qRT-PCR

Total RNA was extracted from cell pellets or tissues with the E.Z.N.A. Total RNA Kit II (Omega Bio-Tek Inc., Norcross, GA). cDNA was transcribed with the High-Capacity cDNA Reverse Transcription Kit (Applied Biosystems, Waltham, MA). Quantitative real-time polymerase chain reaction (qPCR) was run on the ABI 7300 (Applied Biosystems) using TaqMan Fast Advanced PCR Master Mix (Applied Biosystems) or SYBR Green Master Mix (Applied Biosystems). The relative expression was calculated using the $\Delta\Delta C_t$ method with gene expression relative to beta actin or 18S.

RNA sequencing

RNA sequencing was performed on total RNA isolated as described above. RNA libraries were prepared and sequenced using the Illumina Nova Seq and HiSeq platform according to the Illumina Tru-Seq protocol (Novogene, Sacramento, CA). Reference genome

and gene model annotation files were downloaded from genome website browser (NCBI/UCSC/Ensembl) directly. FASTQ files obtained from sequencing were put through fastp to trim adapters and then fastqc for quality analysis. STAR 2.7.1a was then used to align to reference genome (mm10) to trimmed reads after which htseq was used to obtain gene counts. Raw reads were normalized using DESeq2 (1.38.3). Genes with an adjusted *P*-value <0.05 found by DESeq2 were assigned as differentially expressed. Gene set enrichment analysis (GSEA) was performed through the Broad Institute GUI. Normalized counts from DESeq2 from gWAT were input and analyzed with relationship to the Molecular Signature Database (msigdb). Significant Hallmark genes (p <0.05) were graph from both positive and negative normalized enrichment scores (NES). Log2 fold change, p-values and p-adj from differential expression data obtained through deseq2 were loaded into Qiagen's Ingenuity Pathway Analysis (IPA) to look at upstream and downstream regulators. Volcano plots created from differential expression data of pairwise comparison with sham groups being baseline using ggplot2 (3.5). Significant genes from adipogenesis pathway are labeled. Heatmaps were created of genes in the adipogenesis pathway regardless of significance using pheatmap(1.0.12).

Statistical Analysis

Specific statistical tests and sample size for each study is indicated in the figure legends. Error bars in figures show SEM. Statistical analyses were performed using GraphPad Prism (version 9; GraphPad Software Inc), and graphs were built using GraphPad Prism (GraphPad Software Inc) statistical analysis software or R studio (4.2.3) using ggplot (3.5.1). P values are 2 sided with values less than 0.05 regarded as statistically significant.

Data Availability

Further information and resources, including KPC cells and raw data will be shared upon reasonable request to Aaron J. Grossberg (grossber@ohsu.edu).

RESULTS

Adipocytes suppress lipogenesis in response to PDAC-derived factors

Given a large body of literature suggesting that PDAC cachexia is partly driven by increased lipolysis in the adipose tissue, we tested the effect of PDAC cell conditioned media (KPC CM) on lipolysis *in vitro* [21, 22, 38]. We treated differentiated 3T3-L1 cells with control maintenance media, or with KPC CM for 6 days. At this time, we observed decreased lipid droplet accumulation by brightfield microscopy, which was confirmed with Oil Red O (**Figure 1A-B**). Liberated triglyceride (TG) levels, a measure of lipolysis, were significantly lower in the media of KPC CM-treated cells (**Figure 1C**). Correspondingly, mRNA levels of lipolysis enzymes adipose triglyceride lipase (*Atgl*) and lipase E (*Lipe*) were significantly decreased in KPC CM-treated 3T3-L1 cells (**Figure 1D**). To explain the apparent decrease in lipid accumulation without increased lipolysis, we measured the expression of genes associated with lipogenesis: fatty acid synthase (*Fasn*), nuclear receptor subfamily 1 group H member 3 (*Nr1h3*), solute carrier family 2 member 4 (*Slc2a4*), and lipoprotein lipase (*Lpl*). All of these genes were suppressed after KPC CM treatment, indicating that the decreased lipid content in 3T3-L1 cells was due to impaired anabolic activity rather than increased catabolic activity (**Figure 1E**).

PDAC is associated with decreased fat pad mass *in vivo*

We first sought to assess the effects of pancreatic cancer on metabolism by characterizing tissue physiology in a murine orthotopic PDAC model. 12-week-old C57BL/6J

mice with PDAC or sham implantations were fed *ad libitum* with or without a 24h fast once mice reached a moderate cachexia burden (9 days after tumor implantation). Body mass maintained stable among all groups prior to fasting (**Figure 2A**), whereas PDAC mice exhibited a small reduction in food intake (**Figure 2B**) compared to sham controls. EchoMRI body composition analysis of fat mass demonstrated significant decreases in overall adiposity in PDAC animals from baseline to pre-fast due to cachexia progression and reduction in food intake (**Figure 2C**). As expected, between pre- and post-fast, both PDAC and sham animals lost significant overall adiposity (**Figure 2D**). Terminal fat pad mass in fasted PDAC animals was not significantly altered compared to fasted sham mice (**Figure 2E**), indicating that both groups exhibit similar rates of fasting-induced lipolysis. Fasting caused a significant reduction in tumor mass compared to *ad libitum*-fed mice (**Figure 2F**).

PDAC impairs lipolysis and adipogenesis

Based on our findings *in vitro*, we hypothesized that PDAC mice would not exhibit increased lipolysis, which is characteristic of other cachexia models [21, 38]. To measure the rate of adipose tissue catabolism, we performed an *ex vivo* lipolysis study, using gonadal white adipose tissue (gWAT) collected from sham and PDAC mice. We assessed fat pads both in the presence and absence of the beta-adrenergic agonist isoproterenol (10 uM) to determine baseline and stimulated lipolysis[39]. Baseline and isoproterenol-stimulated glycerol release were significantly decreased in PDAC gWAT (**Figure 3A**), demonstrating that PDAC suppresses, rather than enhances, lipolytic rate and capacity. To further characterize the molecular biology of adipocytes during PDAC, we assessed mRNA expression of genes regulating lipolysis and browning in adipose tissue. PDAC mice failed to increase gWAT and inguinal white adipose tissue (iWAT) *Atgl* and *Lipe* expression in response to fasting (**Figure**

3B). We observed similar decreases in browning-associated gene expression, including peroxisome proliferator-activated receptor gamma coactivator 1 alpha (*Pgc1a),* protein domain containing 16 (*Prdm16*), and cell death inducing DFFA like effector a (*Cidea*) in PDAC mice in both *ad libitum* fed and fasted conditions. Uncoupling protein 1 (*Ucp1*), which is also associated with browning, was not significantly increased in gWAT from PDAC mice (**Figure 3B-C**). Therefore, neither enhanced lipolysis nor browning are significant contributors to adipose loss in this model.

PDAC downregulates pathways associated with adipogenesis

To gain further insights into PDAC metabolism from global gene expression analysis, we performed bulk RNA sequencing (RNAseq) on gWAT from sham and PDAC animals. . In gWAT, we identified a total of 572 differentially expressed genes (DEGs) in PDAC versus sham mice, of which 446 were enriched, and 126 were depleted (**Figure 4A, S1**). Pathway analysis referencing the molecular signatures database (MSigDB) hallmark gene set collection revealed increased expression of gene sets associated with cell cycle control (e.g., E2F targets and G2M checkpoints) and inflammation (e.g. TNFa and JAK/STAT3 signaling) and decreased expression of genes linked to adipogenesis, oxidative phosphorylation, and fatty acid metabolism (**Figure 4B**)[40]. Because inhibition of adipogenesis could provide an alternative mechanism for adipose wasting, we plotted all significant DEGs in the adipogenesis gene set and observed nearly universal depletion of these transcripts in PDAC mice (**Figure 4C**). We then validated our RNAseq data by performing qPCR on selected adipogenesis-associated DEGs, revealing consistent downregulation of both adipogenesis and lipogenesis genes (**Figure 4D**). We then repeated qPCR in iWAT to determine whether subcutaneous adipose exhibited the same transcriptomic changes. Transcriptional changes in iWAT were

less dramatic than in gWAT and did not reach significance, with the exception of *Lpl*, which was significantly decreased in PDAC tissue (**Figure 4E**). Together, these results indicate that suppressed transcriptomic programs associated with adipogenesis could account for decreased adipose tissue during cachexia, in the absence of elevated lipolysis.

Adipose tissue anabolism is impaired in orthotopic PDAC mice after refeeding

Based on our results demonstrating downregulation of adipogenic and lipogenic genes in PDAC mice, we next wanted to confirm whether adipose tissue anabolism is functionally impaired in mice implanted with orthotopic PDAC. To do this, wildtype C57BL/6J mice with PDAC or sham implantations were fed *ad libitum* for 9 days, an established timepoint of active cachexia[41], fasted 24h, and then terminated or allowed to re-feed for 24 h. To control for differences in caloric intake, we used a pair-fed refeeding scheme in which sham mice were refed with the average food consumption of the refed PDAC group. Challenging mice with a 24h fast depletes adipose mass equally in PDAC and sham mice (**Figure 2D**), enabling us to assess anabolic restoration of fat mass during a 24 h refeeding period. We observed measured cumulative food intake and daily body mass for the duration of the study (**Figure 5A-B**). Fasting and refeeding did not impact pancreas tumor mass (**Figure S2**). There were no differences in iWAT or gWAT mass in fasted PDAC versus sham mice (**Figure 5C-D**). However, while sham mice regain significant amounts of gWAT and iWAT mass after refeeding, gWAT and iWAT masses in PDAC mice remain equivalent before and after refeeding (**Figure 5C-D**). Refeeding sham mice caused increased gWAT expression of lipogenic *Fasn* and adipogenic genes *Lep* and *Retn*, while these genes remained suppressed in PDAC gWAT (**Figure 5E**). Refed sham iWAT showed increased *Fasn,* but not adipogenic genes, while PDAC iWAT had suppressed expression of both adipogenic and lipogenic genes

(**Figure 5F**). These results confirm that downregulation in pathways mediating adipogenesis are indeed accompanied by impaired adipose tissue anabolism in orthotopic PDAC mice after refeeding.

HuR is overexpressed in orthotopic PDAC fat tissue

Following our observation that adipose tissue anabolism is impaired in PDAC animals, we next sought to understand the mechanism of this phenomenon. We used Ingenuity Pathway Analysis upstream regulator analysis to identify potential candidates that could drive impaired anabolism in PDAC adipose tissue. From the DEGs identified in gWAT of PDAC mice, we found that canonical regulators of adipogenesis, such as troglitazone, fenofibrate, PPARA, and PGC1A, were predicted to be inhibited. Inflammatory cytokines associated with PDAC and cachexia, such as MYD88, IL-6, TNFA, IFNG, and IL-1B, were predicted to be activated. Among other targets that were predicted to be activated but were not typically associated with cachexia was human antigen R (HuR, *ELAVL1*), an RNA-binding protein recently established as a suppressor of adipogenesis[34] (**Figure 6A**). Given the predicted activation of HuR in gWAT and existing literature, we next asked if HuR was more abundant in adipose tissue from PDAC mice. We performed immunohistochemical staining of HuR in formalin-fixed, paraffin-embedded sham and PDAC gWAT, iWAT, pancreas, and muscle tissue. HuR staining was significantly increased in both the gWAT and iWAT of PDAC mice versus sham controls (**Figure 6C-D, S4).** We also observed increased HuR staining in the pancreas, but not skeletal muscle from PDAC mice, as compared to sham controls (**Figure 6B, S3**).

HuR inhibition improves metabolic deficits and restores adipogenesis *in vivo*

Since HuR has been established as driving pro-survival pathways in PDAC, we next wanted to determine if preventing HuR binding to target mRNAs could reverse adipose wasting in PDAC cachexia[35]. To do this, we treated PDAC mice with a selective HuR inhibitor, KH-3, which prevents binding of HuR to its target mRNA sequence[42]. All mice received orthotopic PDAC tumor injections and were fed *ad libitum* then fasted 24h with or without a 24h refeed at mid-cachexia (9 days after injection). In each feeding group, mice were treated with the HuR inhibitor KH-3 (100 mg/kg) or vehicle at 6-, 8-, and 10-days post-injection. Cummulative food intake between vehicle and KH3 groups was not statistically significant prior to fast. KH3 treated PDAC mice gained significantly more weight during refeeding compared to vehicle-treated mice (**Figure 7A-B**). Refeeding was associated with larger tumors in both vehicle and KH-3 groups, likely due to both log growth and the propensity for mice to become dehydrated during fasting (**Figure 7C**). KH-3 treatment itself had no effect on tumor growth over this time interval. KH-3 treatment caused a nonsignificant increase in gWAT mass and significantly increased iWAT mass in refed animals (**Figure 7D-F**). In contrast, vehicle-treated mice did not significantly increase fat pad mass during refeeding. This effect is specific to adipose tissue, as gastrocnemius muscle mass was not changed between fast/refeed, or vehicle/KH-3 treatment (**Figure 7F**). To molecularly test the impact of HuR inhibition on adipogenesis and lipogenesis gene expression, we analyzed gWAT and iWAT tissues by qPCR. KH-3 treatment successfully restored expression of adipogenic (*Cebpa, Adipoq, Lep*, *Retn*) and lipogenic (*Fasn*) genes (**Figure 8A-B, D-E**). HuR inhibition did not impact lipolysis gene expression (*Atgl* and *Lipe*) (**Figure 8C, F**). Thus, we show a role for HuR in adipose tissue metabolism during PDAC-associated cachexia, whereby inhibiting HuR successfully ameliorates adipose tissue wasting *in vivo* by restoring the expression of genes associated with adipogenesis and lipogenesis.

DISCUSSION

This work evaluates the relative contributions of enhanced catabolism and impaired anabolism on fat wasting by investigating adipose tissue response to different nutritional contexts and HuR inhibition in cachectic mice. We demonstrate that our murine model of PDAC cachexia exhibits a near-complete deficit in adipose tissue anabolism in the context of reduced lipolysis, which corroborates a growing set of literature that challenges the dogma that fat wasting occurs as a result of only enhanced catabolism[24-26]. We further identify HuR as a potential molecular mediator of adipogenesis during pancreatic cancer progression. Collectively, these studies support other work describing heterogeneity within cancer-associated cachexia that could have major implications on therapeutic strategies moving forward [13, 43]. In the future, clinical trials may see more therapeutic success if they employ patient selection based on patients' underlying mechanisms of wasting.

Our study implicates the RNA-binding protein HuR in the inhibition of adipogenesis and lipogenesis in adipose tissue. HuR can impact the transcriptome through both RNA binding and HuR-dependent splicing [35]. One documented mechanism of HuR-mediated adipogenesis regulation is via HuR binding to adipogenesis upstream regulator *Pparg*, which suppresses *Adipoq* protein expression in a non-transcriptionally dependent manner [44]. In our RNA sequencing, we did not observe increased HuR expression, although others have documented increased HuR expression in response to nuclear factor-kappa B (NF-κB) signaling[45]. Alternatively, we identified HuR as an upstream regulator based on adipose transcriptomic changes associated with PDAC. In this context, HuR is more likely controlled post-translationally, although further investigation is needed to identify the specific PDAC-associated factors that may activate HuR stability and nuclear translocation [46].

Small molecule antagonists of HuR, such as KH-3, are currently in development and have been found to have anti-tumor effects[35, 47]. In our studies, KH-3 ameliorated anti-fat wasting but also induced severe hemolytic anemia in all treated mice. Tumor size was not impacted by KH3 treatment, likely because of the short period of dosing. However, studies aimed to evaluate tumor growth over 5 weeks documented slower tumor growth and fewer metastases in KH-3-treated mice [48]. In our studies, the anti-cachectic effects of KH-3 were specific to adipose tissue and did not preserve skeletal muscle mass. Although prior studies link muscle and adipose wasting, these models are all characterized by enhanced lipolysis and browning [38]. In our model, adipose and muscle wasting appear to be driven by independent mechanisms. Continued improvement of HuR antagonists could lead to therapeutics that restore anabolic potential in adipose tissue, providing a novel approach to alleviating one symptom of cachexia, while also providing anti-tumor benefits.

In addition to impaired anabolic potential in adipose tissue, our PDAC model also presents suppressed lipolysis. Suppressed lipolysis could contribute to systemic defects in energy utilization in cancer cachexia. Prior work from our group shows that PDAC impairs hepatic lipid oxidation but that this does not result in lipid accumulation or fatty liver [41]. While hepatic metabolic deficits were not HuR dependent, it is possible that impaired lipid mobilization contributes to global metabolic disruption. Further interrogation is needed to understand how improved fat retention through HuR inhibition might impact lipid mobilization and systemic metabolism.

ACKNOWLEDGEMENTS

We thank all members of the Aaron Grossberg and Jonathan Brody labs for their helpful discussion and suggestions. We also would like to thank Dr. Laing Xu (Department of

Molecular Biosciences, University of Kansas, Lawrence, Kansas) for generously providing us with the KH3 compound. Author contributions are: Conceptualization, KP, AJG. Methodology, KP, HM, PP, GM, AC, AJG. Validation, PCAW, KP, HM, BW, PP. Formal Analysis, PCAW, KP, HM, BW, PP, GM, AC, AJG. Investigation, PCAW, KP, HM, BW, PP, GM, AC. Writing—Original Draft, PCAW, BLW. Writing – Review and Editing, PCAW, PP, JB, AJG. Visualization, PCAW, KP, HM, BW, PP, GM, AC. Supervision, JB, AJG. Project Administration, JB, AJG. Funding Acquisition, JB, AJG. All authors approved this manuscript.

Funding: This work was supported by National Cancer Institute grants K99CA286709 (PCAW), R37CA280692 (AJG), R01264133 (AJG), and K08245188 AJG), R01 CA212600 (JRB), U01CA224012-03 (JRB), R21 CA263996 (JRB), AACR Grant-15-90-25-BROD (JRB), the Hirshberg Foundation (JRB), and support from the Brenden Colson Center for Pancreatic Care (AJG, JRB, and PCAW). This work is also supported by the Histopathology Shared Resource for pathology studies (University Shared Resource Program at Oregon Health and Sciences University and the Knight Cancer Institute (P30 CA069533 and P30 CA069533 13S5)).

Conflict of interest: The authors do not declare any conflicts of interest.

Ethical standards: The authors of this manuscript certify that they comply with the ethical guidelines for authorship and publishing in the Journal of Cachexia, Sarcopenia and Muscle.[49] All human and animal studies were approved by the appropriate ethics committees and were therefore performed in accordance with the ethical standards laid down in the 1964 Declaration of Helsinki and its later amendments. All human subjects provided informed consent and any identifying information of individual patients has been omitted.

FIGURE LEGENDS

Figure 1: Adipocytes suppress lipogenesis in response to pancreatic ductal adenocarcinoma-conditioned media. Differentiated 3T3-L1 adipocytes were cultured for 6 days in control or KPC CM, with the exception of the TG assay. **(A)** Brightfield images of differentiated 3T3-L1 cells treated with control media (right) or KPC CM (left). Scale bars represent 200 um. Representative of 3 wells per condition. **(B)** Quantification of Oil Red O staining. N = 4 wells per condition. **(C)** Media triglyceride levels after 24 hours of exposure to control or KPC CM. N=3 wells per condition. **(D)** mRNA expression lipolysis genes N= 3 wells per condition, normalized to 18S expression. **(E)** mRNA expression of lipogenesis genes. N= 3 wells per condition, normalized to 18S expression. Pairwise analyses tested with t-test. $p<0.05$, $^{**}p<0.01$, $^{***}p<0.001$, and $^{****}p<0.0001$.

Figure 2: Pancreatic ductal adenocarcinoma is associated with decreased fat pad mass *in vivo*. Wildtype C57BL/6J mice with PDAC or sham implantations were fed *ad libitum* or fasted 24h at mid-cachexia (9 days after injection). Animals were euthanized 10 or 11 days after tumor implantation following the 24h fast. N= 5 sham, 6 PDAC male mice per feeding condition. **(A)** Daily body mass. Statistically tested with 3-way ANOVA $p<0.0001$ for time, time x fast; $p=0.0073$ for fast; $p=0.0097$ for time x tumor status; $p=0.0167$ for tumor status. **(B)** Cumulative food intake. Statistically tested with 3-way ANOVA $p<0.0001$ for time, time x fast; $p=0.0035$ for time x tumor status. **(C-D)** Body composition changes in total adiposity were characterized at baseline to pre-fast between sham and PDAC mice **(C)**, and at pre- to post-fast **(D)**. MRI analyses were statistically tested with mixed effects model with Fisher's LSD test. **(E)** Terminal gWAT mass. **(F)** Terminal pancreas/tumor mass. 2x2 analyses were statistically tested with two-way ANOVA with Tukey multiple comparisons. $^{*}p<0.05$, $^{**}p<0.01$, and $^{****}p<0.0001$.

Figure 3: Pancreatic ductal adenocarcinoma impairs lipolysis and adipogenesis *in vivo*. **(A)** Measurement of lipolysis (glycerol release) in explants derived from gWAT collected 10 days post tumor implantation. Lipolysis was induced by the agonist isoproterenol (10 μM). N= 6 male mice per group. Statistically tested with two-way ANOVA with uncorrected Fisher's LSD test to compare groups. **(B)** mRNA expression lipolysis genes in gWAT collected 10 days post-implantation from 24h fasted and ad lib mice, normalized to 18S expression. N=5 male mice sham fasted; 3 male, 3 female mice sham ad lib; 6 male mice PDAC fasted; 3 male, 2 female mice PDAC ad lib. **(C)** mRNA expression of lipolysis genes in iWAT collected 11 days post-implantation from ad lib mice, normalized to beta actin expression. N= 4 male mice per group. 2x2 data were statistically tested with two-way ANOVA with Tukey multiple comparisons comparing tumor experimental groups to sham controls. Pairwise comparisons were made with unpaired t test. $^{*}p<0.05$, $^{**}p<0.01$, $^{***}p<0.001$, and $^{****}p<0.0001$.

Figure 4: PDAC downregulates pathways associated with adipogenesis. RNAseq on gWAT from ad lib fed PDAC and sham mice collected 14 days post tumor implantation. N = 2 female, 3 male PDAC; 3 female, 2 male sham. **(A)** Volcano plot of differentially expressed genes in gWAT. Blue dots represent significantly downregulated genes (log2FC < -1 and adj $p<0.05$). while red dots represent significantly upregulated genes (log2FC >1 and adj $p<0.05$). Grey dots are insignificant. Labels denote significant differentially expressed genes from the

Hallmark Adipogenesis pathway. **(B)** Broad Institute GSEA significantly enriched pathways in PDAC gWAT relative to sham gWAT (pathway pval <0.05). Blue is downregulated, red is upregulated. **(C)** Heat map of Hallmark Adipogenesis pathways constituents in PDAC and Sham gWAT. Scale represents row normalized raw counts. **(D)** qPCR validation of adipogenesis and lipolysis genes in in gWAT collected 10 days post-implantation from 24h fasted and ad lib mice. N=5 male mice sham fasted; 3 male, 3 female mice sham ad lib; 6 male mice PDAC fasted; 3 male, 2 female mice PDAC ad lib. Statistically tested with two-way ANOVA with Tukey multiple comparisons comparing tumor experimental groups to sham controls. **(E)** qPCR validation of adipogenesis and lipolysis genes in iWAT from ad lib fed mice collected 11 days post implantation. N = 4 male mice per group. Statistically tested with unpaired t test. *p<0.05, **p<0.01, ***p<0.001, and ****p<0.0001.

Figure 5: Adipose tissue anabolism is impaired in orthotopic PDAC mice after refeeding. Wildtype C57BL/6J mice with PDAC were fed *ad libitum* then fasted 24h or fasted 24h followed by a refeed at mid-cachexia (9 days after injection). Sham mice were pair-fed to PDAC average food intake from 2 days post-implantation until study end. Animals were euthanized 9 or 10 days after tumor implantation following the 24h fast or *ad libitum* refeed. N= 3 male and 3 female mice per group. **(A)** Cumulative food intake. Statistically tested with 3 way ANOVA. P<0.0001 for time, p=0.0344 for time x tumor status. **(B)** Daily body mass. Statistically tested with 3 way ANOVA. P<0.0001 for time, p=0.002 for time x tumor status. **(C)** iWAT mass normalized to initial body mass, normalized to beta actin expression. **(D)** gWAT mass normalized to initial body mass, normalized to beta actin expression. **(E)** mRNA expression of anabolic genes in gWAT. **(F)** mRNA expression of anabolic genes in iWAT. Data represented in C-F were statistically tested with two-way ANOVA with Tukey multiple comparisons comparing tumor experimental groups to sham controls. *p<0.05, and ****p<0.0001.

Figure 6: HuR is overexpressed in PDAC orthotopic pancreas and fat tissue. (A) Selected upstream regulator predictions from Ingenuity Pathway Analysis of differentially expressed genes in gWAT. **(B-D)** Representative images and quantification of immunohistochemical detection of HuR in tissue from PDAC and sham mice. **(B)** Pancreas N=4 male and 4 female mice per group. **(C)** gWAT N=4 male and 4 female mice per group. **(D)** iWAT N= 3 female, 2 male sham and 2 female, 3 male PDAC. Scale bars represent 100 um. Statistically tested with t test. *p<0.05, **p<0.01, ***p<0.001, and ****p<0.0001.

Figure 7: HuR inhibition prevents adipose tissue loss *in vivo*. Wildtype C57BL/6J mice with PDAC were fed *ad libitum* then fasted 24h or fasted 24h followed by a refeed at mid-cachexia (9 days after injection). In each feeding paradigm, groups were treated with either vehicle or the HuR antagonist, KH-3, then euthanized 10 or 11 days after tumor implantation following the 24h fast or *ad libitum* refeed. Vehicle-treated mice were pair-fed to the KH-3 treated group's average food intake from 8 days post-implantation until study end. N = 7 male mice per group. **(A)** Cumulative food intake, statistically tested as an unpaired t test of vehicle vs KH3 treatment at day 9 (prior to fast) p =0.1121. **(B)** Change in body weight after refeeding, statistically tested with unpaired *t* test. **(C)** Terminal pancreas mass. **(D)** Terminal gWAT mass. **(E)** Terminal iWAT mass. **(F)** Terminal gastrocnemius mass. 2x2 analyses were statistically tested with two-way ANOVA with Tukey multiple comparisons*p<0.05, and **p<0.01.

514 **Figure 8: HuR inhibition partially restores adipogenesis and lipogenesis *in vivo*. (A)**
515 mRNA expression of Adipogenesis genes in gWAT, normalized to beta actin expression. **(B)**
516 mRNA expression of lipogenesis genes in gWAT. **(C)** mRNA expression of lipolysis genes in
517 gWAT. **(D)** mRNA expression of Adipogenesis genes in iWAT, normalized to beta actin
518 expression. **(E)** mRNA expression of lipogenesis genes in iWAT. **(F)** mRNA expression of
519 lipolysis genes in iWAT. Data were statistically tested with two-way ANOVA with Tukey
520 multiple comparisons correction. N = 7 male mice per group. *p<0.05, **p<0.01, ***p<0.001,
521 and ****p<0.0001.
522

523

REFERENCES

1. Tisdale MJ. Biology of cachexia. J Natl Cancer Inst. 1997;89:1763-73. doi:10.1093/jnci/89.23.1763

2. Grossberg AJ, Scarlett JM, Marks DL. Hypothalamic mechanisms in cachexia. Physiol Behav. 2010;100:478-89. doi:10.1016/j.physbeh.2010.03.011

3. Baracos VE, Martin L, Korc M, Guttridge DC, Fearon KCH. Cancer-associated cachexia. Nat Rev Dis Primers. 2018;4:17105. doi:10.1038/nrdp.2017.105

4. Olson B, Marks DL. Pretreatment Cancer-Related Cognitive Impairment-Mechanisms and Outlook. Cancers (Basel). 2019;11:doi:10.3390/cancers11050687

5. von Haehling S, Anker MS, Anker SD. Prevalence and clinical impact of cachexia in chronic illness in Europe, USA, and Japan: facts and numbers update 2016. J Cachexia Sarcopenia Muscle. 2016;7:507-9. doi:10.1002/jcsm.12167

6. von Haehling S, Anker SD. Cachexia as a major underestimated and unmet medical need: facts and numbers. J Cachexia Sarcopenia Muscle. 2010;1:1-5. doi:10.1007/s13539-010-0002-6

7. Fearon K, Strasser F, Anker SD, Bosaeus I, Bruera E, Fainsinger RL, et al. Definition and classification of cancer cachexia: an international consensus. Lancet Oncol. 2011;12:489-95. doi:10.1016/S1470-2045(10)70218-7

8. Fearon KC, Glass DJ, Guttridge DC. Cancer cachexia: mediators, signaling, and metabolic pathways. Cell Metab. 2012;16:153-66. doi:10.1016/j.cmet.2012.06.011

9. Tisdale MJ. Cachexia in cancer patients. Nat Rev Cancer. 2002;2:862-71. doi:10.1038/nrc927

546 10. Aoyagi T, Terracina KP, Raza A, Matsubara H, Takabe K. Cancer cachexia, mechanism
547 and treatment. World J Gastrointest Oncol. 2015;7:17-29. doi:10.4251/wjgo.v7.i4.17
548 11. Fearon K, Arends J, Baracos V. Understanding the mechanisms and treatment options
549 in cancer cachexia. Nat Rev Clin Oncol. 2013;10:90-9. doi:10.1038/nrclinonc.2012.209
550 12. Mueller TC, Burmeister MA, Bachmann J, Martignoni ME. Cachexia and pancreatic
551 cancer: are there treatment options? World J Gastroenterol. 2014;20:9361-73.
552 doi:10.3748/wjg.v20.i28.9361
553 13. Kays JK, Shahda S, Stanley M, Bell TM, O'Neill BH, Kohli MD, et al. Three cachexia
554 phenotypes and the impact of fat-only loss on survival in FOLFIRINOX therapy for pancreatic
555 cancer. Journal of cachexia, sarcopenia and muscle. 2018;9:673-84.
556 14. Mantovani G, Maccio A, Lai P, Massa E, Ghiani M, Santona MC. Cytokine activity in
557 cancer-related anorexia/cachexia: role of megestrol acetate and medroxyprogesterone
558 acetate. Semin Oncol. 1998;25:45-52.
559 15. Straub RH, Cutolo M, Buttgereit F, Pongratz G. Energy regulation and neuroendocrine-
560 immune control in chronic inflammatory diseases. J Intern Med. 2010;267:543-60.
561 doi:10.1111/j.1365-2796.2010.02218.x
562 16. Argiles JM, Busquets S, Toledo M, Lopez-Soriano FJ. The role of cytokines in cancer
563 cachexia. Curr Opin Support Palliat Care. 2009;3:263-8. doi:10.1097/SPC.0b013e3283311d09
564 17. MacDonald N, Easson AM, Mazurak VC, Dunn GP, Baracos VE. Understanding and
565 managing cancer cachexia. J Am Coll Surg. 2003;197:143-61. doi:10.1016/S1072-
566 7515(03)00382-X

18. Carson JL, Hernandez M, Jaspers I, Mills K, Brighton L, Zhou H, et al. Interleukin-13 stimulates production of nitric oxide in cultured human nasal epithelium. In Vitro Cell Dev Biol Anim. 2018;54:200-4. doi:10.1007/s11626-018-0233-y

19. Haslett PA. Anticytokine approaches to the treatment of anorexia and cachexia. Semin Oncol. 1998;25:53-7.

20. Moldawer LL, Copeland EM, 3rd. Proinflammatory cytokines, nutritional support, and the cachexia syndrome: interactions and therapeutic options. Cancer. 1997;79:1828-39.

21. Das SK, Eder S, Schauer S, Diwoky C, Temmel H, Guertl B, et al. Adipose triglyceride lipase contributes to cancer-associated cachexia. Science. 2011;333:233-8.

22. Petruzzelli M, Schweiger M, Schreiber R, Campos-Olivas R, Tsoli M, Allen J, et al. A switch from white to brown fat increases energy expenditure in cancer-associated cachexia. Cell metabolism. 2014;20:433-47.

23. Taylor J, Uhl L, Moll I, Hasan SS, Wiedmann L, Morgenstern J, et al. Endothelial Notch1 signaling in white adipose tissue promotes cancer cachexia. Nature Cancer. 2023;4:1544-60.

24. Langer HT, Ramsamooj S, Dantas E, Murthy A, Ahmed M, Ahmed T, et al. Restoring adiponectin via rosiglitazone ameliorates tissue wasting in mice with lung cancer. Acta Physiologica. 2024;e14167.

25. Jang HJ, Kim HY, Lyu JH, Muthamil S, Shin UC, Kim HS, et al. Bee (Apis mellifera L. 1758) wax restores adipogenesis and lipid accumulation of 3T3-L1 cells in cancer-associated cachexia condition. Food Science & Nutrition. 2024;

26. Tien S-C, Chang C-C, Huang C-H, Peng H-Y, Chang Y-T, Chang M-C, et al. Exosomal miRNA 16-5p/29a-3p from pancreatic cancer induce adipose atrophy by inhibiting adipogenesis and promoting lipolysis. Iscience. 2024;27:

590 27. Cook KB, Kazan H, Zuberi K, Morris Q, Hughes TR. RBPDB: a database of RNA-
591 binding specificities. Nucleic Acids Res. 2011;39:D301-8. doi:10.1093/nar/gkq1069
592 28. Gerstberger S, Hafner M, Tuschl T. A census of human RNA-binding proteins. Nat Rev
593 Genet. 2014;15:829-45. doi:10.1038/nrg3813
594 29. Pihlajamaki J, Lerin C, Itkonen P, Boes T, Floss T, Schroeder J, et al. Expression of the
595 splicing factor gene SFRS10 is reduced in human obesity and contributes to enhanced
596 lipogenesis. Cell Metab. 2011;14:208-18. doi:10.1016/j.cmet.2011.06.007
597 30. Brosch M, von Schonfels W, Ahrens M, Nothnagel M, Krawczak M, Laudes M, et al.
598 SFRS10--a splicing factor gene reduced in human obesity? Cell Metab. 2012;15:265-6; author
599 reply 7-9. doi:10.1016/j.cmet.2012.02.002
600 31. Huot ME, Vogel G, Zabarauskas A, Ngo CT, Coulombe-Huntington J, Majewski J, et al.
601 The Sam68 STAR RNA-binding protein regulates mTOR alternative splicing during
602 adipogenesis. Mol Cell. 2012;46:187-99. doi:10.1016/j.molcel.2012.02.007
603 32. Chou CF, Lin YY, Wang HK, Zhu X, Giovarelli M, Briata P, et al. KSRP ablation
604 enhances brown fat gene program in white adipose tissue through reduced miR-150
605 expression. Diabetes. 2014;63:2949-61. doi:10.2337/db13-1901
606 33. Dai N, Zhao L, Wrighting D, Kramer D, Majithia A, Wang Y, et al. IGF2BP2/IMP2-
607 Deficient mice resist obesity through enhanced translation of Ucp1 mRNA and Other mRNAs
608 encoding mitochondrial proteins. Cell Metab. 2015;21:609-21. doi:10.1016/j.cmet.2015.03.006
609 34. Siang DTC, Lim YC, Kyaw AMM, Win KN, Chia SY, Degirmenci U, et al. The RNA-
610 binding protein HuR is a negative regulator in adipogenesis. Nat Commun. 2020;11:213.
611 doi:10.1038/s41467-019-14001-8

612 35. Finan JM, Sutton TL, Dixon DA, Brody JR. Targeting the RNA-binding protein HuR in
613 cancer. Cancer Research. 2023;83:3507-16.
614 36. Michaelis KA, Zhu X, Burfeind KG, Krasnow SM, Levasseur PR, Morgan TK, et al.
615 Establishment and characterization of a novel murine model of pancreatic cancer cachexia. J
616 Cachexia Sarcopenia Muscle. 2017;8:824-38. doi:10.1002/jcsm.12225
617 37. Schweiger M, Eichmann TO, Taschler U, Zimmermann R, Zechner R, Lass A.
618 Measurement of lipolysis. Methods Enzymol. 2014;538:171-93. doi:10.1016/B978-0-12-
619 800280-3.00010-4
620 38. Rupert JE, Narasimhan A, Jengelley DH, Jiang Y, Liu J, Au E, et al. Tumor-derived IL-6
621 and trans-signaling among tumor, fat, and muscle mediate pancreatic cancer cachexia.
622 Journal of Experimental Medicine. 2021;218:e20190450.
623 39. Schweiger M, Eichmann TO, Taschler U, Zimmermann R, Zechner R, Lass A.
624 Measurement of lipolysis. In: Elsevier; 2014. pp. 171-93.
625 40. Liberzon A, Birger C, Thorvaldsdóttir H, Ghandi M, Mesirov JP, Tamayo P. The
626 molecular signatures database hallmark gene set collection. Cell systems. 2015;1:417-25.
627 41. Arneson-Wissink PC, Mendez H, Pelz K, Dickie J, Bartlett AQ, Worley BL, et al. Hepatic
628 signal transducer and activator of transcription-3 signalling drives early-stage pancreatic
629 cancer cachexia via suppressed ketogenesis. J Cachexia Sarcopenia Muscle. 2024;15:975-88.
630 doi:10.1002/jcsm.13466
631 42. Wu X, Gardashova G, Lan L, Han S, Zhong C, Marquez RT, et al. Targeting the
632 interaction between RNA-binding protein HuR and FOXQ1 suppresses breast cancer invasion
633 and metastasis. Commun Biol. 2020;3:193. doi:10.1038/s42003-020-0933-1

634 43. Fearon Kenneth CH, Glass David J, Guttridge Denis C. Cancer Cachexia: Mediators,
635 Signaling, and Metabolic Pathways. Cell Metabolism. 2012;16:153-66.
636 doi:10.1016/j.cmet.2012.06.011
637 44. Hwang JS, Lee WJ, Hur J, Lee HG, Kim E, Lee GH, et al. Rosiglitazone-dependent
638 dissociation of HuR from PPAR-γ regulates adiponectin expression at the posttranscriptional
639 level. The FASEB Journal. 2019;33:7707-20. doi:10.1096/fj.201802643r
640 45. Kang MJ, Ryu BK, Lee MG, Han J, Lee JH, Ha TK, et al. NF-κB Activates
641 Transcription of the RNA-Binding Factor HuR, via PI3K-AKT Signaling, to Promote Gastric
642 Tumorigenesis. Gastroenterology. 2008;135:2030-42.e3. doi:10.1053/j.gastro.2008.08.009
643 46. Grammatikakis I, Abdelmohsen K, Gorospe M. Posttranslational control of HuR
644 function. Wiley Interdisciplinary Reviews: RNA. 2017;8:e1372.
645 47. Huang Z, Liu S, Tang A, Wu X, Aube J, Xu L, et al. Targeting RNA-binding protein HuR
646 to inhibit the progression of renal tubular fibrosis. Journal of Translational Medicine.
647 2023;21:428.
648 48. Dong R, Chen P, Polireddy K, Wu X, Wang T, Ramesh R, et al. An RNA-Binding
649 Protein, Hu-antigen R, in Pancreatic Cancer Epithelial to Mesenchymal Transition, Metastasis,
650 and Cancer Stem Cells. Mol Cancer Ther. 2020;19:2267-77. doi:10.1158/1535-7163.Mct-19-
651 0822
652 49. von Haehling S, Coats AJ, Anker SD. Ethical guidelines for publishing in the Journal of
653 Cachexia, Sarcopenia and Muscle: update 2021. Wiley Online Library; 2021. pp. 2259-61.
654

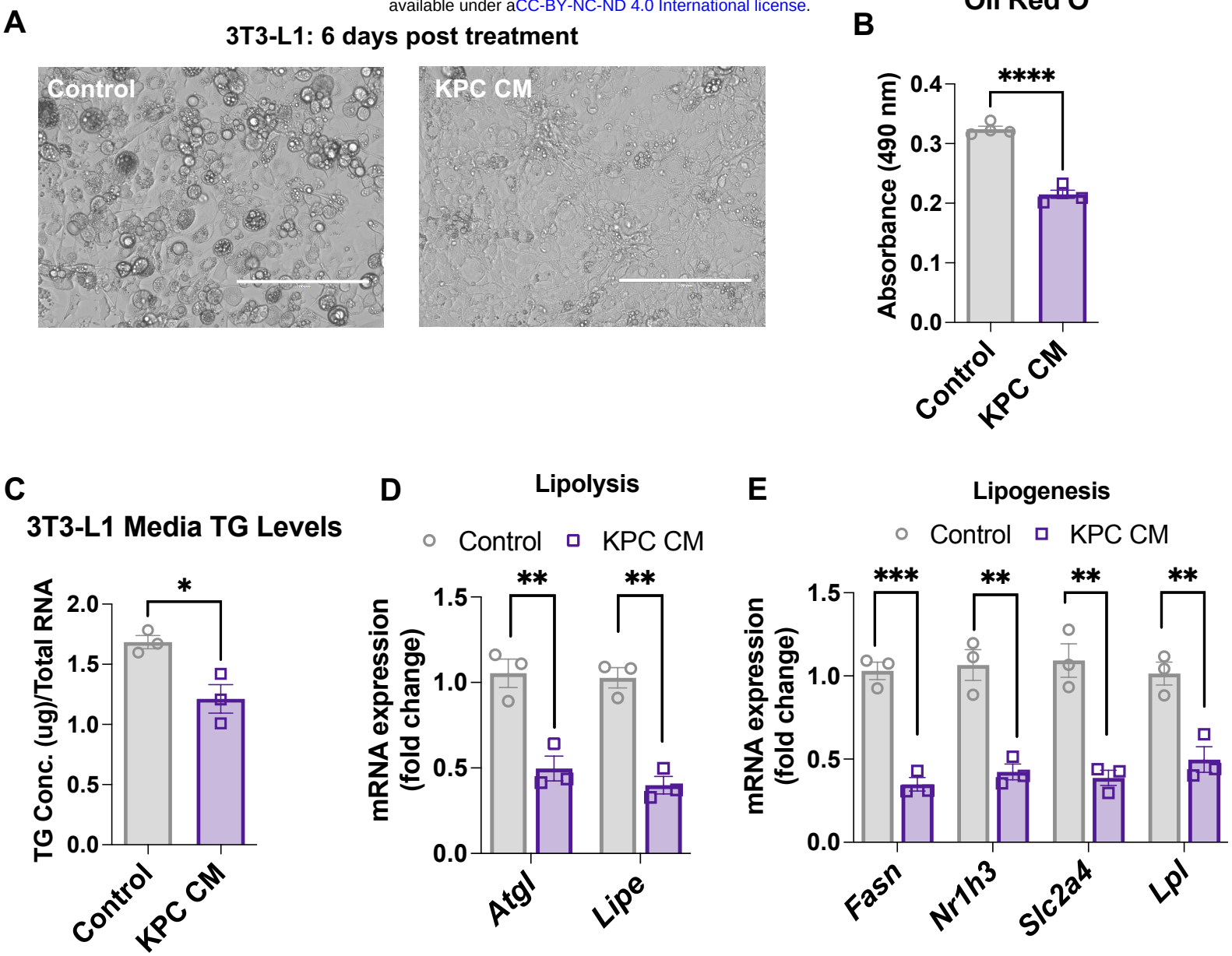

Figure 1

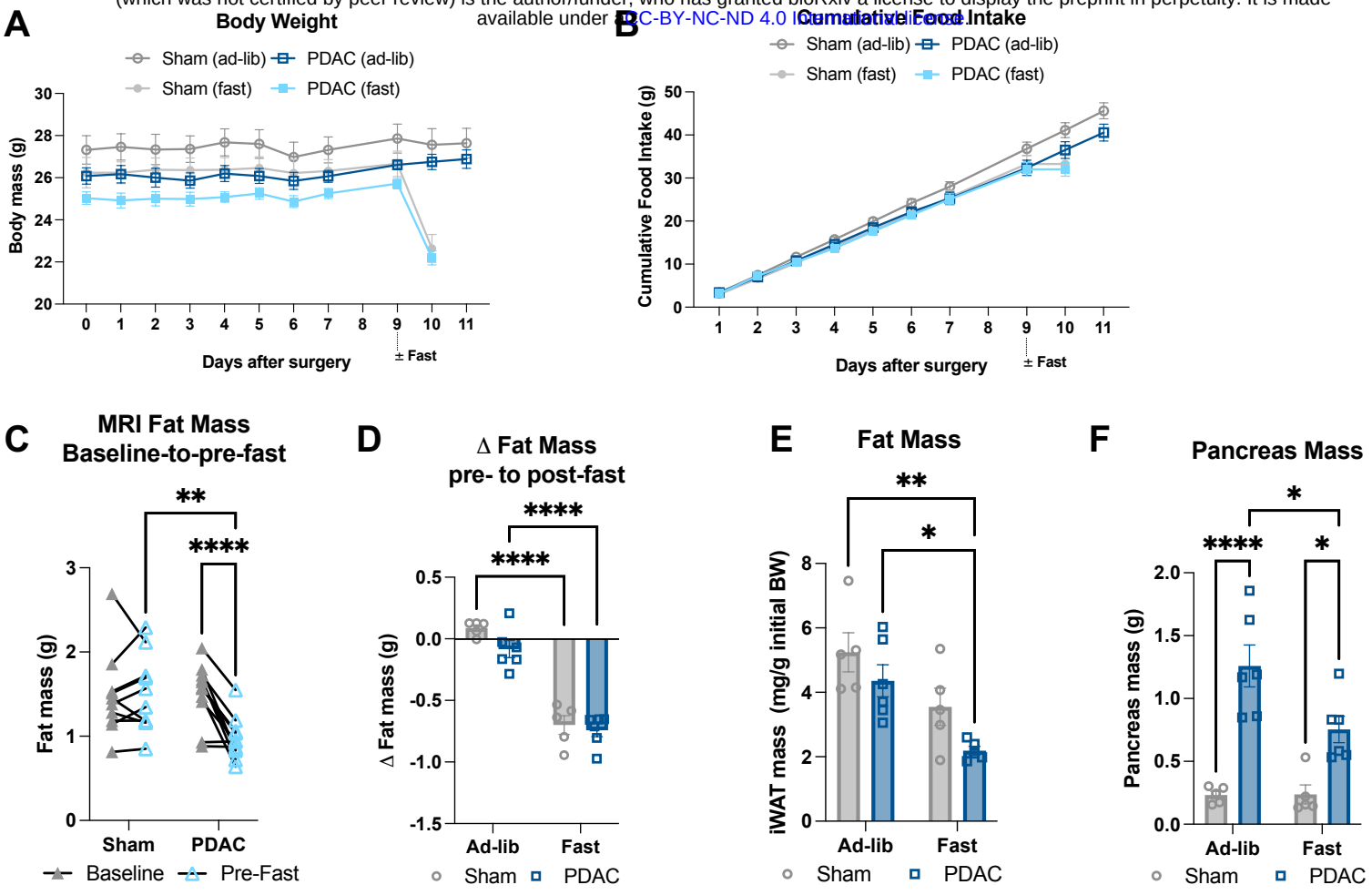

Figure 2

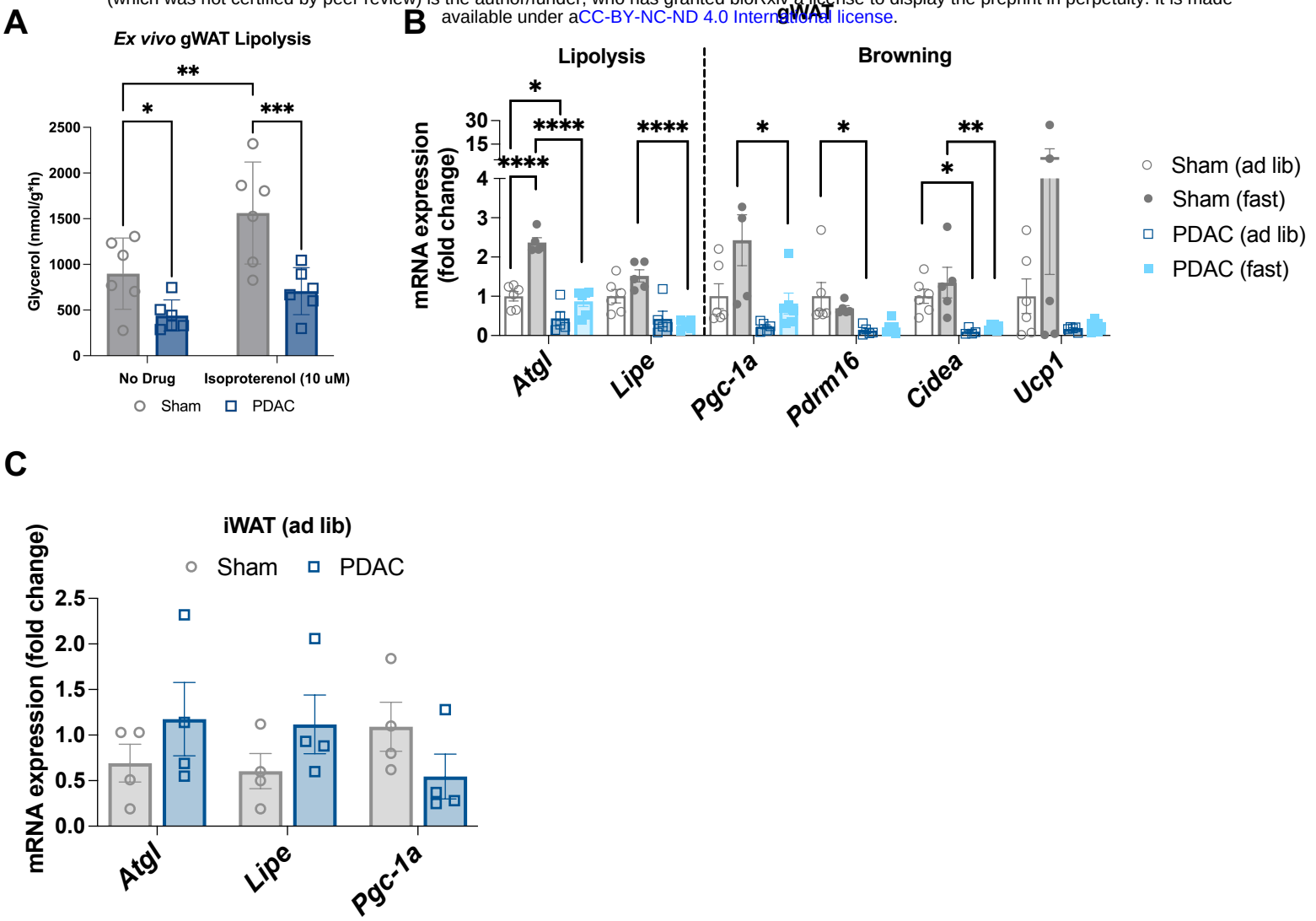

Figure 3

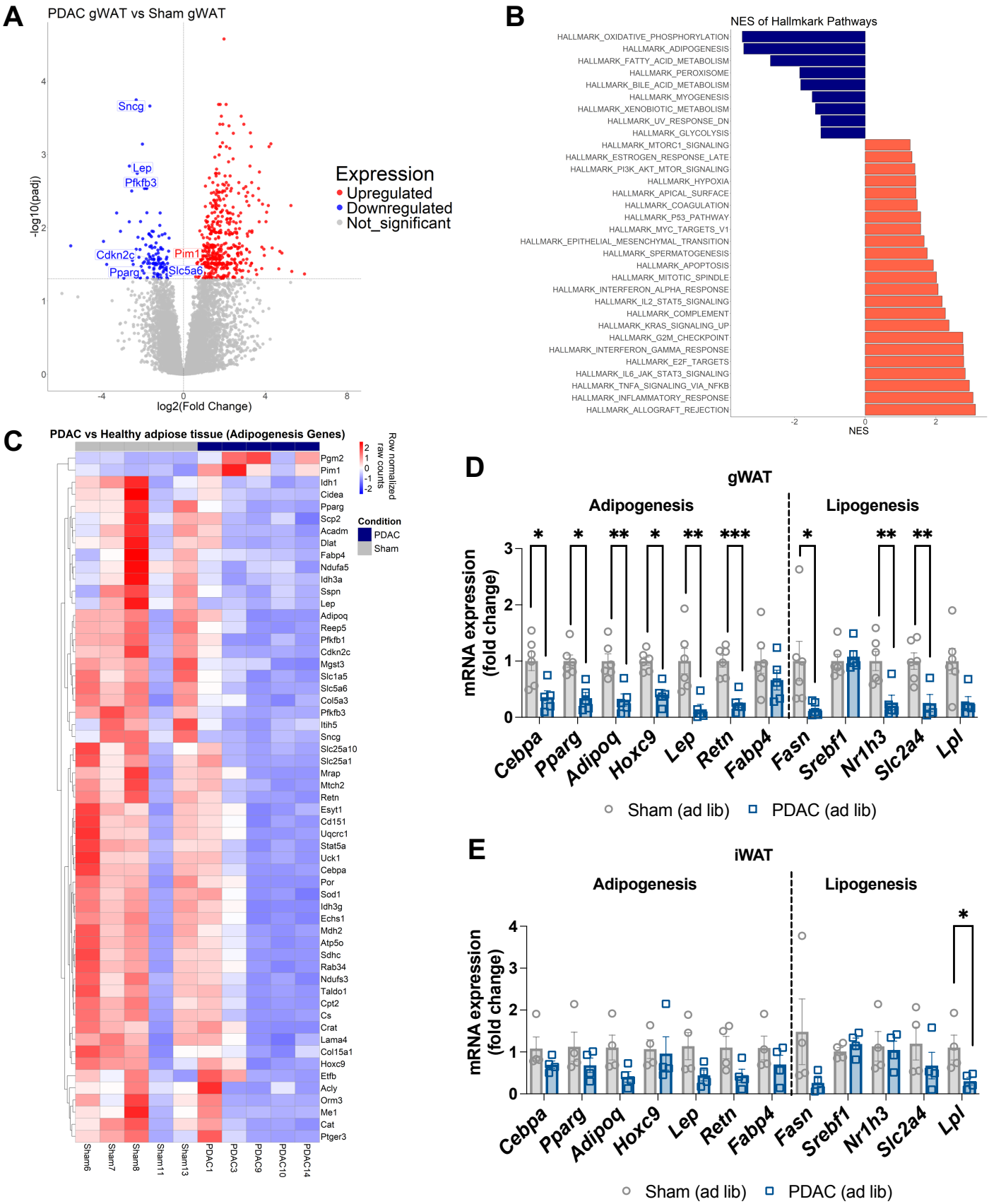

Figure 4

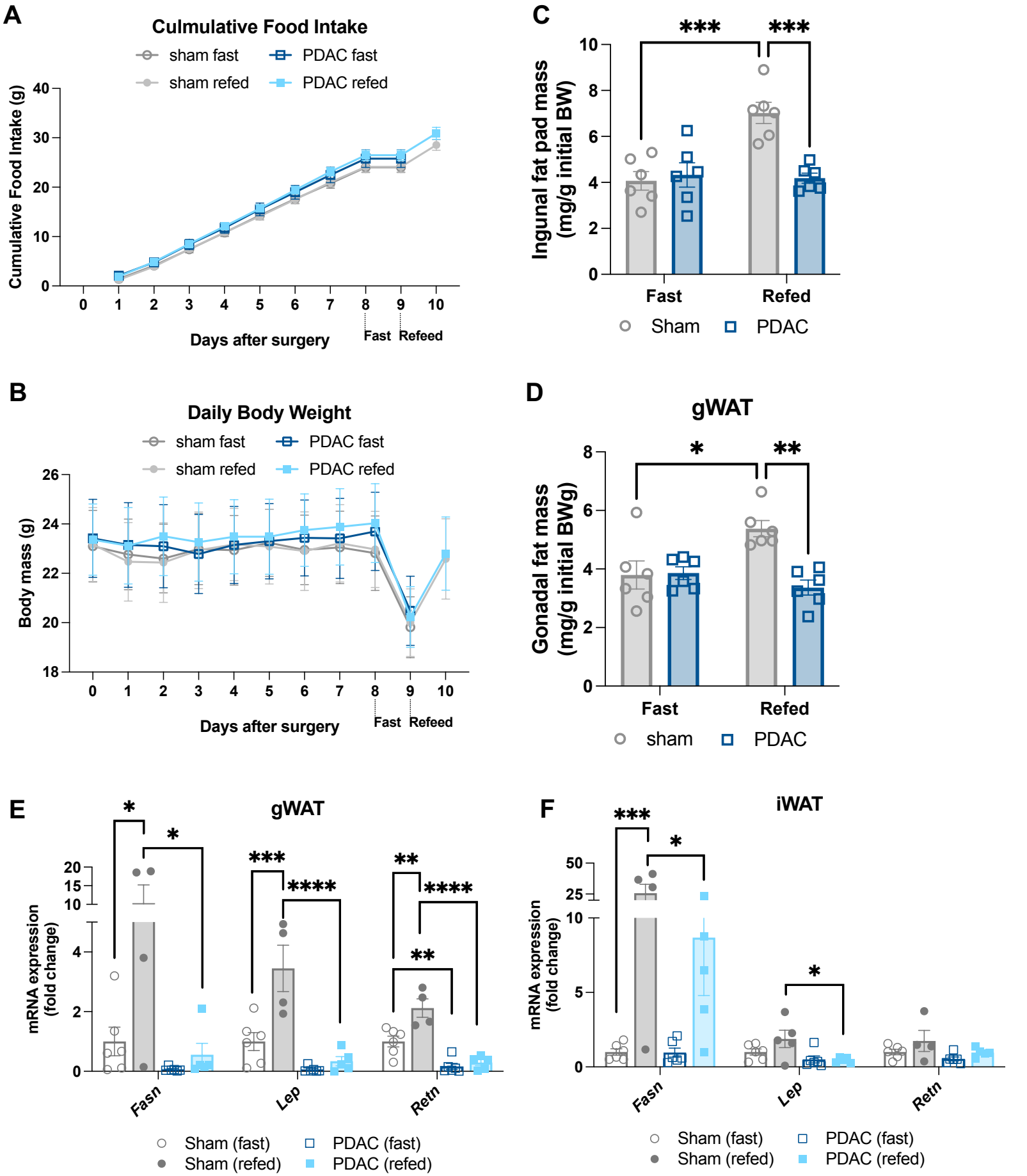

Figure 5

A

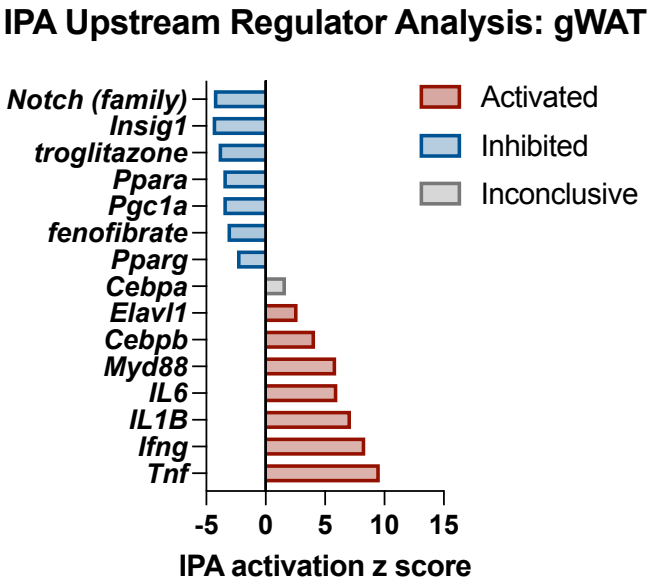

B

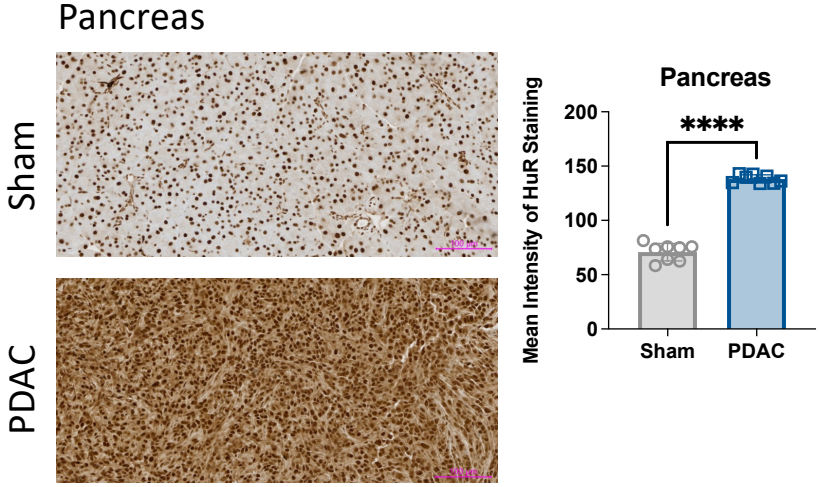

C

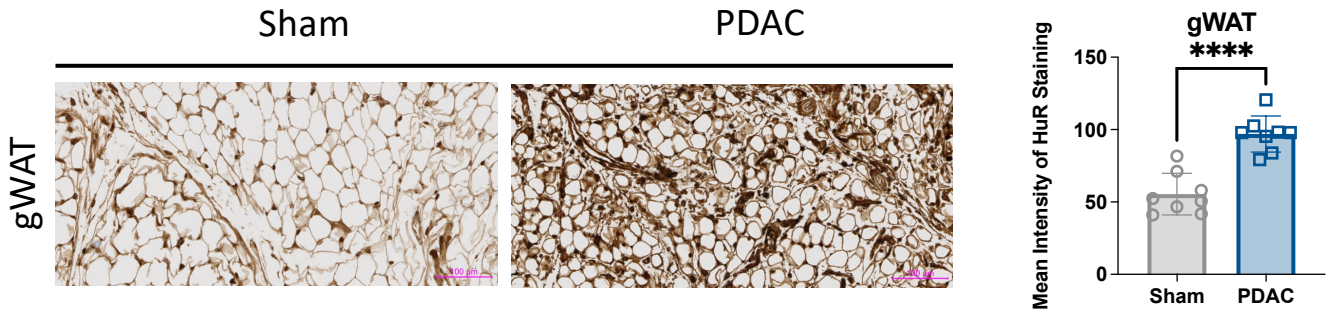

D

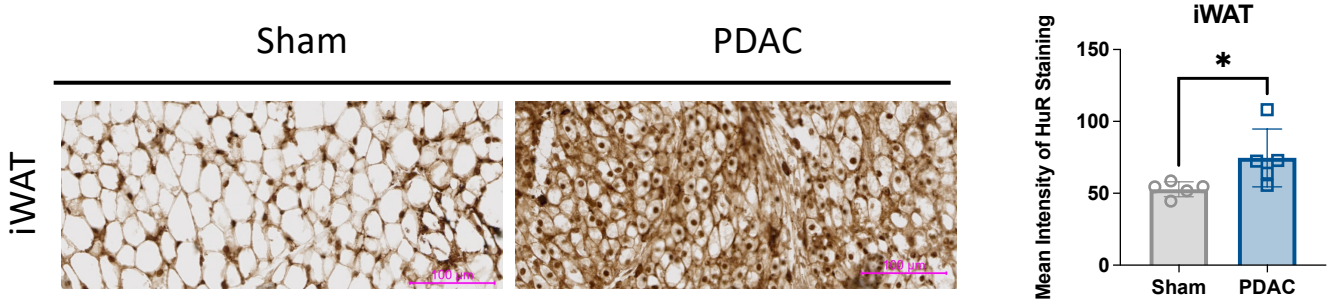

Figure 6

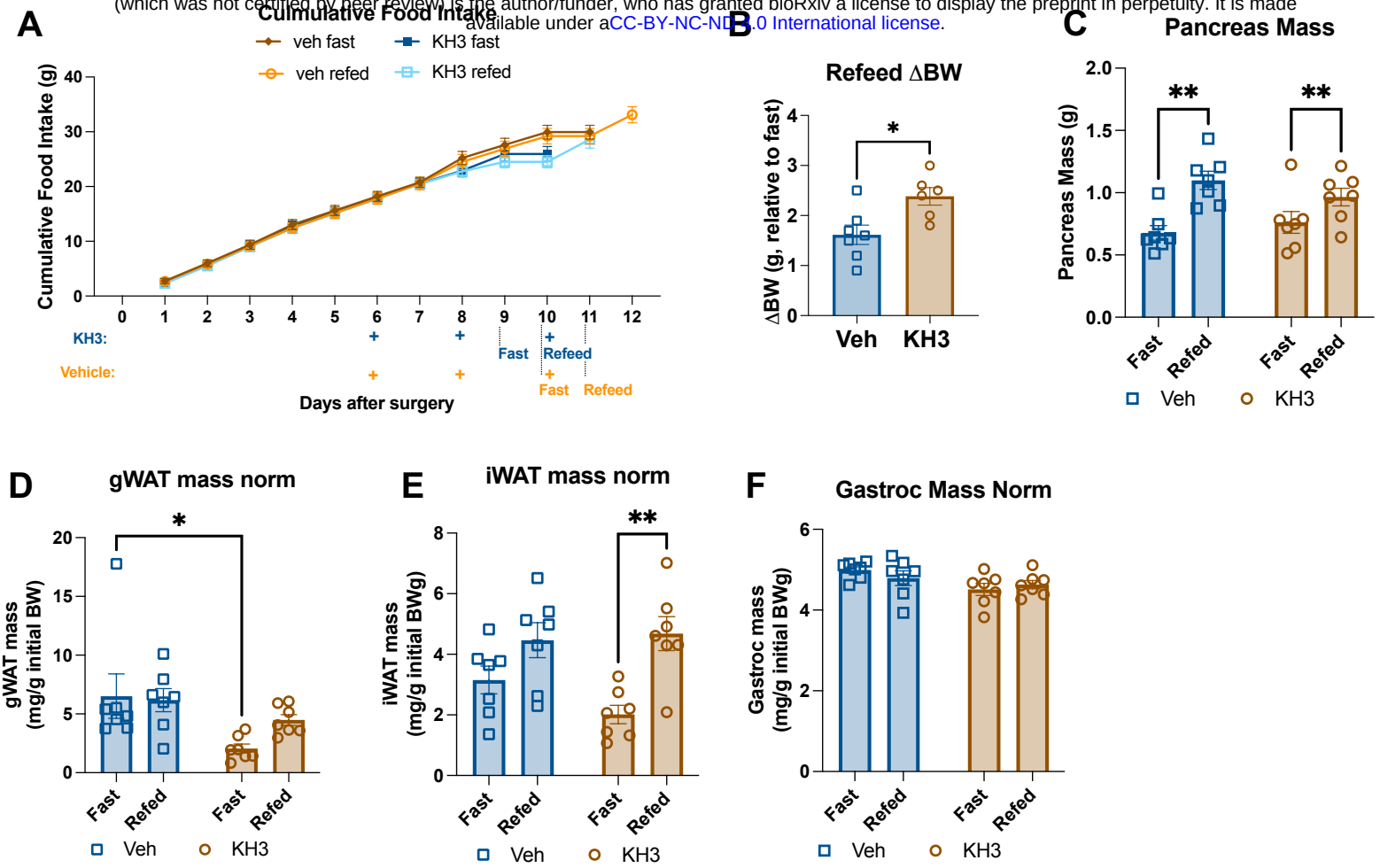

Figure 7

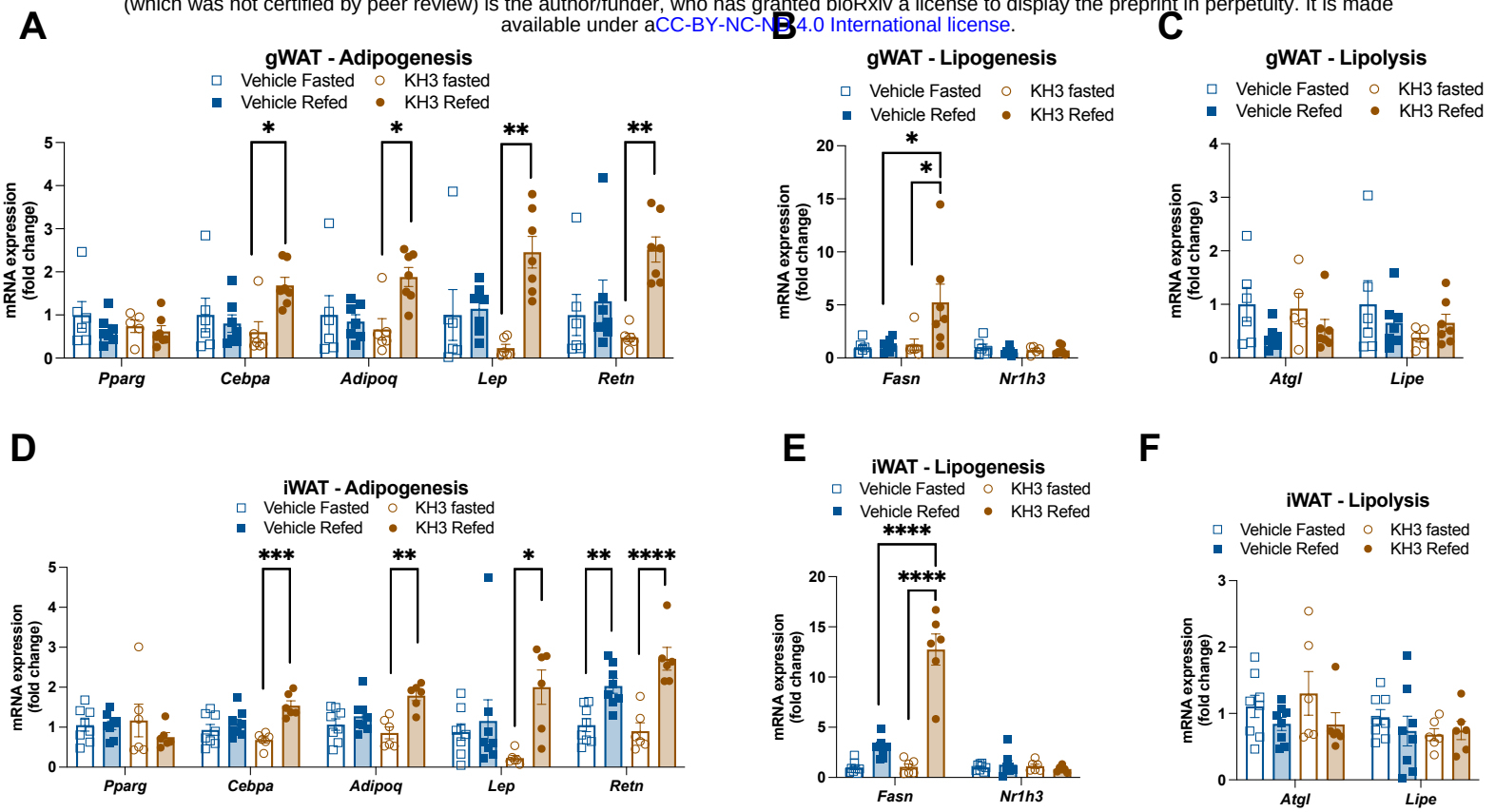

Figure 8